

Evolution of Micropits on Large Terraces of the Si(111) Surface during High-Temperature Annealing

A. S. Petrov^{a,*}, S. V. Sitnikov^a, S. S. Kosolobov^b, and A. V. Latyshev^{a,c}

^a Institute of Semiconductor Physics, Siberian Branch, Russian Academy of Sciences, Novosibirsk, 630090 Russia

^b Skolkovo Institute of Science and Technology, Skolkovo, Moscow oblast, 143026 Russia

^c Novosibirsk State University, Novosibirsk, 630090 Russia

*e-mail: alexey_petrov@isp.nsc.ru

Received October 22, 2018; revised October 29, 2018; accepted October 29, 2018

Abstract—The transformation of micropits on large terraces of the Si(111) surface containing no vicinal atomic steps has been investigated by in situ ultrahigh-vacuum reflection electron microscopy upon thermal annealing of the substrate in the range of 1200–1400°C. A procedure for the formation of micropits on large terraces of the Si(111) surface with the application of focused-ion-beam (Ga⁺) technology has been proposed. It has been found that the micropit decay kinetics varies upon reaching the critical radius R_{crit} , which is caused by the activation of nucleation of two-dimensional vacancy islands on the micropit bottom. A theoretical model describing variations in the lateral sizes of the micropit both before and after reaching R_{crit} has been proposed. Based on analysis of the found temperature dependence of the nucleation frequencies of two-dimensional vacancy pits on the micropit bottom, the effective energy of nucleation of a vacancy island has been determined to be 4.1 ± 0.1 eV.

DOI: 10.1134/S1063782619040237

1. INTRODUCTION

Ultrahigh-vacuum high-temperature annealing is a widespread method for forming atomically clean surfaces of silicon. Herewith, the morphology of a surface slightly misoriented from the crystallographic face is always determined by the density of steps and their direction [1]. The application of lithographic methods makes it possible to control the distribution of atomic steps, for example, by forming regions containing two-dimensional vacancy islands at the vertex of a pedestal [2–4]. Using surface structurization, important quantitative parameters that characterize atomic processes during sublimation and epitaxial growth in the temperature range of 830–1300°C have been determined [2, 3, 5]. An increase in the rate of atomic processes hampers the observation of positions of separate atomic steps at higher temperatures [3]. Information on atomic processes in the case of high-temperature thermal annealing or epitaxial growth can be extracted from analysis of the transformation kinetics of lithographically structured surfaces [6, 7]. However, the theoretical description of experimental investigations of the transformation of lithographic surfaces formed on a vicinal crystal surface is hampered because of the necessity to take into account their interaction with vicinal steps, dislocations, and other surface defects [8, 9].

In this work, a procedure for studying the micropit decay kinetics on large terraces of the Si(111) surface

containing no vicinal structures during thermal annealing of the substrate by an alternating electric current is proposed. The goal of our work is to determine the mass transport mechanism during micropit transformation on large terraces of the Si(111) surface at 1200–1400°C.

2. EXPERIMENTAL

Standard samples with dimensions $7 \times 1.1 \times 0.3$ mm were cut from a phosphorus-doped silicon wafer (111) oriented with a misorientation of the surface of less than 0.01° . The sample, after chemical cleaning with petroleum ether, was placed into an ion-beam etching installation with high-energy argon ions (PIPS Model 691), where a hollow (macropit) up to 0.8 mm in diameter and up to 2 μm in depth was formed on its surface. Then the sample was preliminarily annealed in the chamber of an ultrahigh-vacuum reflection electron microscope (UHV REM) at a temperature higher than 1300°C in order to form an atomically clean silicon surface. A wide terrace up to 100 μm in diameter restricted by concentric atomic steps was formed at the macropit bottom during thermal annealing at ultrahigh-vacuum conditions [10–12]. The annealed sample was extracted from the UHV REM chamber and further structurization of the surface was performed by the focused-ion-beam (Ga⁺) method based on a CrossBeam 1540 XB (Carl Zeiss)

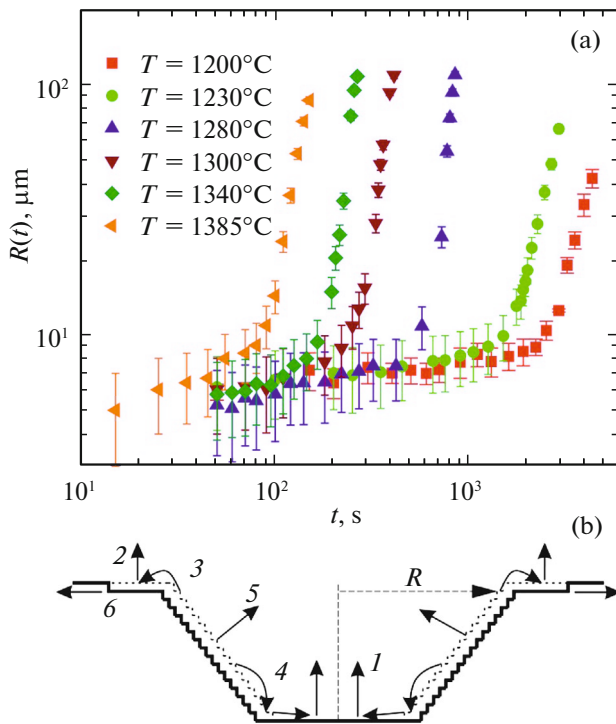


Fig. 1. (a) Dependences of the micropit radius on the annealing time at various temperatures. (b) Schematic image of a micropit during thermal annealing. (1, 2) Desorption of atoms from terraces at the bottom and around it; (3, 4) the escape of atoms from the micropit edge on the adjoining terrace and on the bottom; (5) the desorption of atoms from the micropit edge; and (6) step detachment from the micropit edge.

installation [13]. A micropit with lateral sizes of $5 \times 5 \mu\text{m}$ and 500 nm in depth was formed at the macropit center on the wide terrace surface.

The thus prepared samples were placed into REM ultrahigh-vacuum chamber to perform experimental investigations. To clean the surface with removal of the native oxide layer and contaminants associated with the procedure of sample preparation, annealing was performed at $T \approx 1300^\circ\text{C}$ for 50 s. The substrate temperature was monitored using an optical pyrometer. The sample temperature was additionally calibrated by the $(7 \times 7) \rightarrow (1 \times 1)$ superstructure phase transition, which is observed on the Si(111) surfaces at $T = 830^\circ\text{C}$ [14]. The formation of the Si(111)– (7×7) structural reconstruction was detected by the appearance of additional superstructural reflections at the electron microdiffraction pattern of the sample surface. Experimental investigations into the morphology of the surface with micropits were performed at 1200–1400°C. The samples were heated in the UHV REM chamber by AC passing. This made it possible to exclude the influence of the electromigration of silicon atoms adsorbed on the surface, which could lead to the redistribution of atomic steps, the formation of step eche-

lons, and surface coarsening on the micropit transformation [1].

The UHV REM procedure makes it possible to visualize separate atomic steps, two-dimensional and three-dimensional islands, surface reconstructions, and structural surface defects, as well as to perform in situ experiments on epitaxial growth and sublimation. The REM operating principle is based on the fact that the high-energy electron beam (100 keV) is incident on the sample surface at Bragg angles on the order of several angular degrees. So far as the incidence angle of electrons on the surface is small, they penetrate into the sample bulk to a depth not exceeding units of nanometers; correspondingly, elastically scattered electrons carry information only on the surface layers. The intensity of the diffracted beams is determined by the structure of several atomic planes near the crystal surface, which determines the high REM sensitivity to the surface layer structure.

The UHV REM does not make it possible to directly form an image of the entire surface of the wide terrace ($\sim 100 \mu\text{m}$ in diameter) containing the micropit. In order to analyze the entire terrace surface, step-by-step annealing is performed as follows. The sample was annealed at the specified temperature T and rapidly cooled with a cooling rate of 400 K/s to 900°C . The sequence of REM images containing all regions of a wide terrace was recorded at a substrate temperature of 900°C , and then the step with high-temperature annealing was repeated. The REM images were combined in a graphics editor to form a panoramic pattern of the entire surface containing the micropit.

It is noteworthy that a specific feature of the UHV REM method is image compression in the electron-beam incidence direction by a factor of ~ 60 . One pixel in the transverse direction corresponds to 6.3 nm, while in the longitudinal direction, it corresponds to 382.5 nm. The longitudinal and transverse micropit sizes were measured in panoramic REM patterns, and their average value was accepted as a micropit diameter at a specific annealing instant.

3. RESULTS

The variation in the radius of micropits R (Fig. 1b) is measured during thermal annealing in the temperature range of 1200–1400°C for 17 samples. Figure 1a shows the dependence of R for the annealing time t for some of them. It is seen that the plot slope increases for all temperatures during annealing with an increase in R , which corresponds to an increase in the rate of motion of the micropit edge. Let us consider the mass transport processes inside the micropit and in its immediate proximity in detail.

When heating the Si(111) sample to high temperatures ($>1200^\circ\text{C}$), active sublimation proceeds, which occurs in several stages according to classical notions developed in [15]. These are detachment of the atom

from the step, its diffusion over the terrace, and subsequent desorption. Figure 1b shows a schematic image of the micropit; arrows 1 and 2 show fluxes of atoms desorbing from terraces on the bottom and around the micropit, respectively. The replenishment of atoms on the terraces occurs due to their detachment from the micropit walls (Fig. 1b, processes 3 and 4), which leads to material redistribution at the micropit edge and its shift. Direct sublimation of the material from the micropit edge is also possible (Fig. 1b, process 5). It is noteworthy that the square micropit shape is transformed into a round one in a short time interval of initial annealing due to these processes.

At the same time, single atomic steps are periodically detached from the micropit edge (Fig. 1b, process 6), which leads to a decrease in the number of atomic steps at the micropit edge. The micropit has a depth of ~ 1500 monoatomic steps at the initial instant. The decay rate increases with a decrease in the micropit depth at constant atomic flux from the micropit edge.

The maximal micropit edge is limited by the diameter of the macropit bottom, on which it was formed. It was established experimentally that the micropit decay rate starts to slow upon the approach of its edges to the inner macropit perimeter at a distance on the order of $20 \mu\text{m}$ or smaller. Such experimental points are excluded from theoretical consideration because of the complexity of taking into account the interaction between the micropit and macropit.

A terrace containing no atomic steps, which increases during micropit decay, is formed at the micropit bottom during thermal annealing. A two-dimensional vacancy island is nucleated upon the terrace reaching critical sizes R_{crit} , which agrees with the results of works [16–18] published previously. A system of concentric vacancies is formed at the terrace bottom with the further increase in the micropit size, in the center of which, a new vacancy island is periodically nucleated. Figure 2 shows two REM images of micropits with sizes on the order of (a) 50 and (b) $100 \mu\text{m}$, which are formed by the above-described method. Arrows with digit 2 denote concentric vacancy islands, while small (5–10 μm) two-dimensional vacancy islands are formed on the terrace between them upon rapid cooling from temperatures above 1180°C according to the data of [17, 19].

4. DISCUSSION OF RESULTS

Let us represent the micropit on the surface in the form of a cylindrical hollow of radius R and depth H , around which there is a terrace with the width L (Fig. 3a). As was shown above, the atomic step detaches during sublimation and moves from the micropit edge. Let us note that L is the maximal terrace size. As far as the characteristic time of varying the micropit sizes is considerably longer than the sub-

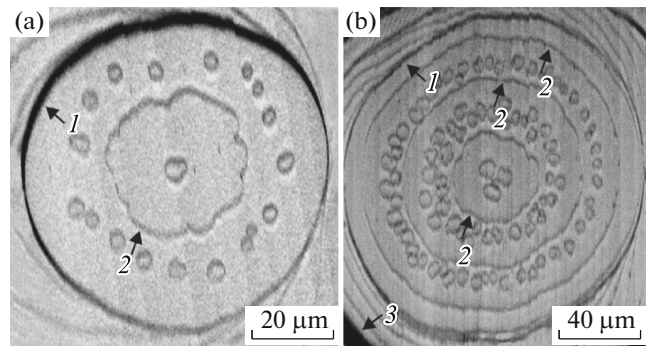


Fig. 2. REM images of the micropit after annealing (a) for 120 s at $T = 1385^\circ\text{C}$ and (b) for 255 s at $T = 1340^\circ\text{C}$. (1) Micropit edge, (2) concentric atomic step restricting the vacancy island, and (3) inner micropit edge.

limination time of one surface bilayer at the annealing temperatures used in the experiment, we can average the sublimation process in the model over time. Here-with, atoms from the micropit walls come to the micropit bottom, on an adjoining terrace with the size L or are directly desorbed in free space (Fig. 3a). It is accepted to consider in the model that adatoms desorbed from the micropit bottom are replenished by adatoms escape on the terrace from the micropit walls, while adatoms desorbed from the adjoining terrace are replenished adatoms escaped both from the micropit edge and from the step. Because of the relatively small magnitude of L when compared with microstructure sizes, we can accept with sufficient accuracy that half of atoms on the adjoining terrace escaped from the micropit edge, and the remaining half escaped from the step limiting this terrace.

Let us write a balance equation for the fluxes of the material being desorbed from the surface and escaping from the micropit edge:

$$\left(\pi R^2(t) + 2\pi R(t)H(t) + \pi \frac{(R(t) + L)^2 - R^2}{2} \right) \times v_1 h_0 dt = 2\pi R(t)H(t)dR(t), \quad (1)$$

where h_0 is the height of one bilayer of the Si(111) surface with a density of $1.56 \times 10^{15} \text{ atom cm}^{-2}$; $R(t)$, $H(t)$ are the micropit radius and depth, respectively; and v_1 is the sublimation frequency of one surface bilayer determined as follows:

$$v_1 = v_0 e^{-\frac{E_{\text{sub}}}{k_B T}}, \quad (2)$$

where v_0 is the frequency of atomic oscillations, E_{sub} is the activation energy of sublimation, k_B is the Boltzmann constant, and T is the temperature. The left side of Eq. (1) corresponds to the flux of the material, which is desorbed from the micropit bottom with the area $\pi R^2(t)$ (Fig. 3a, flux j_1), from its lateral surface $2\pi R(t)H(t)$ with the area (Fig. 3a, flux j_2), and from

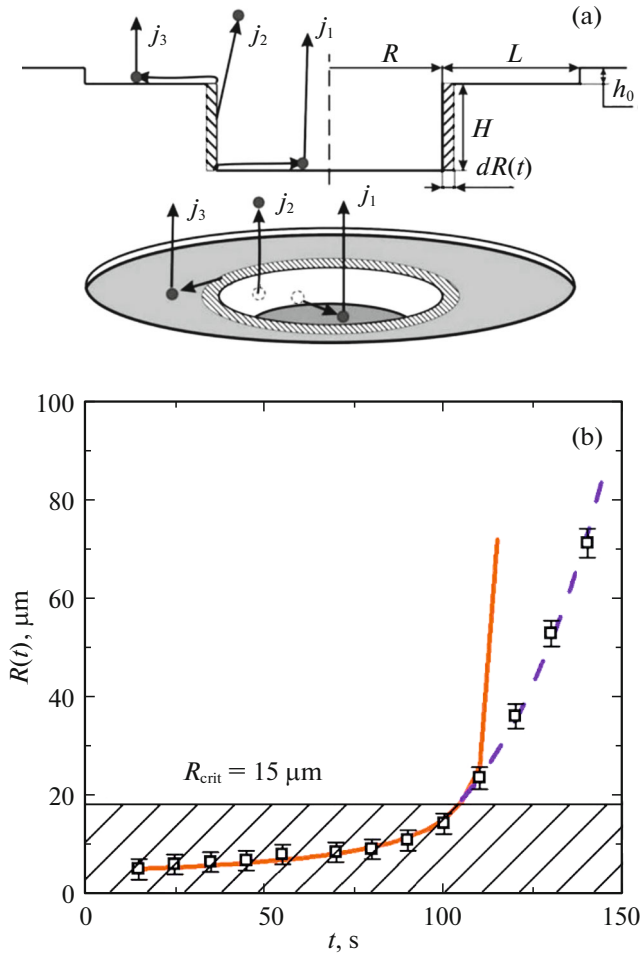


Fig. 3. (a) Schematic image of the micropit during decay; j_1, j_2 , and j_3 are fluxes of atoms, which are desorbed from the micropit bottom, from the side surface, and from the adjoining terrace, respectively. (b) Experimental dependence of the micropit radius depending on the annealing time at $T = 1385^\circ\text{C}$; the solid line is the $R(t)$ theoretical dependence not allowing for the nucleation of vacancy islands; the dashed line is the $R(t)$ theoretical dependence allowing for the nucleation of vacancy islands at $R > R_{\text{crit}}$.

half of the adjoining terrace with the area $\frac{\pi(R(t) + L)^2 - R^2}{2}$ (Fig. 3a, flux j_3).

The right side of the equation determines the flux of the compensating material from the micropit edge. The magnitude of $R(t)$ increases during the escape of atoms from the lateral wall by quantity dR denoted by hatching in Fig. 3a. The micropit depth can be determined as $H(t) \approx H_0 - h_0 t \nu_1$, where H_0 is the initial micropit depth and h_0 is the atomic-step height on the Si(111) surface (0.314 nm).

Equation (1) was solved numerically with known initial parameters such as the micropit radius and depth. The terrace width L was measured during the experiment and was $1.5 \mu\text{m}$ on average. The variable

parameter was the sublimation frequency ν_1 . Varying this parameter, we have obtained theoretical $R(t)$ values of for various temperatures. Figure 3b shows the typical experimental dependence of the micropit radius on the annealing time at $T = 1385^\circ\text{C}$ combined with the theoretical curve (solid line). The theoretical model well describes the experimental results at small pit radii, while a deviation is observed at sizes larger than $20 \mu\text{m}$. Herewith, the micropit in the experiment decays slower than in the theoretical model.

The cause of the divergence between the theory and experiment is the nucleation of two-dimensional vacancy islands at the micropit bottom, which is activated when the micropit reaches the critical size. This process slows the decrease in the micropit depth, which in turn causes a decrease in its decay rate. To take into account the nucleation processes, Eq. (1) should be supplemented with the additional parameter $h_0 t \nu_2$, where ν_2 is the nucleation frequency of vacancy islands. Equation (1) will take the following form:

$$\left(\pi R^2(t) + 2\pi R(t)H(t) + \pi \frac{L(R(t) + L)}{2} \right) \nu_1 h_0 dt \quad (3)$$

$$= 2\pi R(t)(H_1(t) - h_0 t \nu_1 + h_0 t \nu_2) dR(t), \quad t > \tau,$$

where $H_1 \approx H_0 - h_0 t \nu_1$ is the micropit depth at the instant τ corresponding to reaching of the critical radius of micropit for the nucleation of vacancy islands. The nucleation frequency ν_2 is the variable parameter in balance equation (3), which is applicable for region $R(t) > R_{\text{crit}}$. Taking into account nucleation processes, the theoretical model describes well the experimental results of micropit decay during annealing (dashed line in Fig. 3b).

The frequencies ν_1 and ν_2 of the sublimation of one bilayer from the Si(111) surface and nucleation of the vacancy island, respectively, were determined from the approximation of experimental results by Eqs. (1) and (3) using the least-squares method in the temperature range of $1200\text{--}1400^\circ\text{C}$ (Fig. 4). The errors of quantities ν_1 and ν_2 are caused by a difference between the theoretical and experimental value of $R(t)$ and were equal from 3 to 15%. The frequencies determined in this work agree with the previously found values in the temperature range of $1100\text{--}1300^\circ\text{C}$ [19] and follow a single activation dependence with an energy of $E_{\text{sub}} = 3.9 \pm 0.1 \text{ eV}$ for sublimation and $E_{\text{nuc}} = 4.1 \pm 0.1 \text{ eV}$ for the nucleation of vacancy islands. The sublimation energy agrees with the published data found by various methods at temperatures up to 1350°C — $4.1 \pm 0.2 \text{ eV}$ [1, 19], 4.09 eV [20], $4.3 \pm 0.3 \text{ eV}$ [2, 21], and $4.1 \pm 0.5 \text{ eV}$ [22].

It is noteworthy that some authors suggested the incomplete surface melting of the silicon crystal at substrate temperatures above 1290°C [23, 24]. The authors of these works assume the presence of a new surface phase with other energy parameters, which determine both mass transport over the surface and material desorption from the surface into free space.

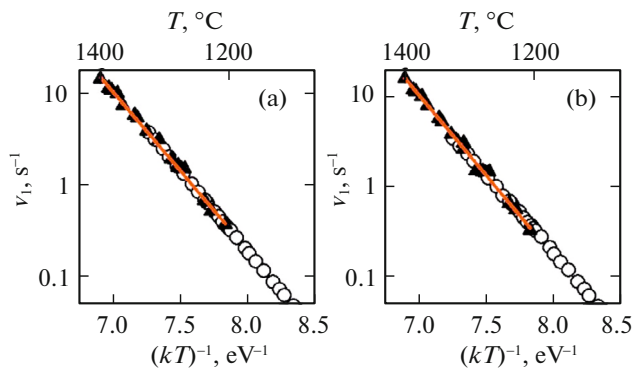


Fig. 4. Temperature dependences of (a) the sublimation frequencies and (b) the nucleation of two-dimensional vacancy islands; square filled points show the experimental results of this work, the solid line denotes approximation by the exponential function, and round points show the values found in [19].

The results of our investigation showed that the sublimation energy of silicon from the Si(111) surface is invariable with an increase in the substrate temperature above 1290°C and, correspondingly, the transition of the surface layer into the partially molten state is improbable. It is also known from publications that surface melting occurs for metals, for example, on the Pd(110) surface [25, 26]. However, this phenomenon was not found for Pd(111), which was attributed to a high reticular density of this orientation [27].

5. CONCLUSIONS

Micropit decay processes on large terraces of the Si(111) surface during annealing by AC resistive heating in the temperature range 1200–1400°C have been investigated by the UHV REM technique. A noticeable decrease in the micropit-decay kinetics upon reaching micropit critical lateral size is found. The critical size is determined by the onset of nucleation of vacancy islands at the micropit bottom. A simple theoretical model, which describes well the variations in the lateral micropit sizes and takes into account two kinetic modes—without and with the nucleation of vacancy islands—has been proposed. The temperature dependences of the sublimation frequencies from the surface and nucleation of vacancy islands have been found. Based on the analysis of these dependences, the activation energies of the sublimation and nucleation of vacancy islands 3.9 ± 0.1 and 4.1 ± 0.1 eV, respectively, have been obtained.

ACKNOWLEDGMENTS

This work is performed using equipment of the JUC “Nanostructures”; model construction is supported by the Russian Scientific Foundation, project no. 14-22-00143.

REFERENCES

1. A. V. Latyshev and A. L. Aseev, *Monatomic Steps on the Silicon Surface* (Sib. Otdel. RAN, Novosibirsk, 2006) [in Russian].
2. Y. Homma, H. Hibino, and T. Ogino, *Phys. Rev. B* **58**, 146 (1998).
3. K. L. Man, A. B. Pang, and M. S. Altman, *Surf. Sci.* **601**, 4669 (2007).
4. S. V. Sitnikov, S. S. Kosolobov, and A. V. Latyshev, *Semiconductors* **51**, 203 (2017).
5. S. V. Sitnikov, A. V. Latyshev, and S. S. Kosolobov, *J. Cryst. Growth* **457**, 196 (2015).
6. H. C. Kan, T. Kwon, and R. J. Phaneuf, *Phys. Rev. B* **77**, 205401 (2008).
7. T. Kwon, R. J. Phaneuf, and H. Kan, *Appl. Phys. Lett.* **88**, 071914 (2006).
8. K. Li, N. Pradeep, S. Chikkamaranahalli, G. Stan, R. Attota, J. Fu, and R. Silver, *J. Vac. Sci. Technol. B* **29**, 41806 (2011).
9. K.-C. Chang and J. M. Blakely, *Surf. Sci.* **591**, 133 (2005).
10. H.-C. Jeong and E. D. Williams, *Surf. Sci. Rep.* **34**, 171 (1999).
11. T. Ogino, H. Hibino, and Y. Homma, *Crit. Rev. Solid State Mater. Sci.* **24**, 227 (1999).
12. S. V. Sitnikov, S. S. Kosolobov, D. V. Shchegolov, and A. V. Latyshev, RF Patent No. 2453874 (2012).
13. C. A. Volkert and A. M. Minor, *MRS Bull.* **32**, 389 (2007).
14. K. Takayanagi, Y. Tanishiro, M. Takahashi, and S. Takahashi, *J. Vac. Sci. Technol. A* **3**, 1502 (1985).
15. A. Pimpinelli and J. Villain, *Phys. A (Amsterdam, Neth.)* **204**, 521 (1994).
16. Y. Homma, N. Aizawa, and T. Ogino, *Jpn. J. Appl. Phys.* **35**, L241 (1996).
17. Y. Homma, H. Hibino, T. Ogino, and N. Aizawa, *Phys. Rev. B* **55**, R10237 (1997).
18. S. V. Sitnikov, S. S. Kosolobov, and A. V. Latyshev, *Surf. Sci.* **633**, L1 (2015).
19. S. V. Sitnikov, S. S. Kosolobov, and A. V. Latyshev, *Vestn. NGU* **11**, 94 (2016).
20. A. B. Pang, K. L. Man, M. S. Altman, T. J. Stasevich, F. Szalma, and T. L. Einstein, *Phys. Rev. B* **77**, 115424 (2008).
21. C. Alfonso, J. C. Heyraud, and J. J. Metois, *Surf. Sci. Lett.* **291**, 745 (1993).
22. J. M. Bermond, J. C. Heyraud, and C. Alfonso, *Surf. Sci.* **331–333**, 855 (1995).
23. Y. Fukaya and Y. Shigeta, *Phys. Rev. Lett.* **85**, 5150 (2000).
24. V. Ignatescu and J. M. Blakely, *Surf. Sci.* **601**, 5459 (2007).
25. J. Frenken, P. Maree, and J. van der Veen, *Phys. Rev. B* **34**, 7506 (1986).
26. G. Grubel, D. Gibbs, D. Zehner, D. Abernathy, A. Sandy, and S. Mochrie, *Surf. Sci.* **287–288**, 842 (1993).
27. B. Pluis, J. Frenken, and J. van der Veen, *Phys. Rev. Lett.* **59**, 2678 (1987).

Translated by N. Korovin